

# Probing the mass and anisotropy of the Milky Way gaseous halo: Sight-lines toward Mrk 421 and PKS2155-304

A. Gupta and S. Mathur<sup>1</sup>

*Astronomy Department, Ohio State University, Columbus, OH 43210, USA*

agupta@astronomy.ohio-state.edu

M. Galeazzi

*Physics Department, University of Miami, Coral Gables, FL 33124, USA*

Y. Krongold

*Instituto de Astronomia, Universidad Nacional Autonoma de Mexico Mexico City, (Mexico)*

## ABSTRACT

We recently found that the halo of the Milky Way contains a large reservoir of warm-hot gas that contains a large fraction of the missing baryons from the Galaxy. The average physical properties of this circumgalactic medium (CGM) are determined by combining average absorption and emission measurements along several extragalactic sightlines. However, there is a wide distribution of both, the halo emission measure and the O VII column density, suggesting that the Galactic warm-hot gaseous halo is anisotropic. We present *Suzaku* observations of fields close to two sightlines along which we have precise O VII absorption measurements with *Chandra*. The column densities along these two sightlines are similar within errors, but we find that the emission measures are different:  $0.0025 \pm 0.0006 \text{ cm}^{-6} \text{ pc}$  near the Mrk 421 direction and  $0.0042 \pm 0.0008 \text{ cm}^{-6} \text{ pc}$  close to the PKS2155-304 sightline. Therefore the densities and pathlengths in the two directions must be different, providing a suggestive evidence that the warm-hot gas in the CGM of the Milky Way is not distributed uniformly. However, the formal errors on derived parameters are too large to make such a claim. In the Mrk 421 direction we derive the density of  $1.6^{+2.6}_{-0.8} \times 10^{-4} \text{ cm}^{-3}$  and pathlength of  $334^{+685}_{-274} \text{ kpc}$ . In the PKS2155-304 direction we measure the gas density of  $3.6^{+4.5}_{-1.8} \times 10^{-4} \text{ cm}^{-3}$  and path-length of  $109^{+200}_{-82} \text{ kpc}$ . Thus the density

---

<sup>1</sup>Center for Cosmology and Astro-Particle Physics, The Ohio State University, Columbus, OH 43210

and pathlength along these sightlines are consistent with each other within errors. The average density and pathlength of the two sightlines are similar to the global averages, so the halo mass is still huge, over 10 billion solar masses. With more such studies, we will be able to better characterize the CGM anisotropy and measure its mass more accurately. We can then compare the observational results with theoretical models and investigate if/how the CGM structure is related to the larger scale environment of the Milky Way.

We also show that the Galactic disk makes insignificant contribution to the observed O VII absorption; a similar conclusion was also reached by Henley and Shelton (2013) about the emission measure. We further argue that any density inhomogeneity in the warm-hot gas, be it from clumping, from the disk, or from a non-constant density gradient, would strengthen our result in that the Galactic halo path-length and the mass would become larger than what we estimate here. As such, our results are conservative and robust.

## 1. Introduction

Late-type galaxies in the Local Universe are missing more than 70% of their baryonic mass. A large fraction of these missing baryons are likely embedded in the low density, warm-hot gas extended over 100 kpc in the circumgalactic medium (CGM) or galactic halo (Silk 1977; White & Rees 1978; Sommer-Larsen 2006). Alternatively, the missing baryons from galaxies may have escaped from the potential wells of galaxies but reside in their parent groups or clusters (e.g., Humphrey et al. 2011). Finally, the missing baryons can be in the form of local warm-hot intergalactic filament (WHIM, Cen & Ostriker 1999; Mathur et al. 2003; Nicastro et al. 2002, 2003). Whether in the CGM or in their group or cluster medium, these missing baryons are expected to be in a warm-hot gas phase at temperatures between  $10^5 - 10^7$  K.

The UV metal absorption lines through external galaxies provide strong evidence for the presence of the warm gas ( $T < 10^6$  K) in the CGM. Recently Tumlinson et al. (2011) probed CGM of 42 galaxies with O VI absorption lines. They found that the CGM around star-forming galaxies is extended, to over 100 kpc and the mass content in the ionized gas is over  $10^9 M_{\odot}$ . But the mass of the gas probed by UV absorption lines is significantly below what is required to account for the galactic missing baryons; it falls short by an order of magnitude.

The warm-hot gas at temperatures  $10^6 - 10^7$  K can only be detected in the soft X-ray band, probed by even more highly ionized metals such as O VII. There are observational

evidences that spiral galaxies have reservoirs of ionized warm-hot gas in the CGM. Recently Williams et al. (2013) investigated intervening X-ray absorption line systems toward H2356-309 observed by Buote et al. (2009), Fang et al. (2010) and Zappacosta et al. (2012). They found that three of the four absorption systems originate within virial radii of nearby galaxies along the sightline with projected distances of 100s of kpc, implying that these intervening X-ray absorption lines probe CGMs of external galaxies instead of the WHIM. Anderson et al. (2013) detected X-ray emission around isolated galaxies observed in the ROSAT All-Sky Survey (RASS) extended out to 50 kpc. They estimate the median masses of the hot gas extending out to 200 kpc around early-type and luminous galaxies of  $1.5 \times 10^{10} M_{\odot}$  and  $3.3 \times 10^{10} M_{\odot}$ , respectively. There are also other reports of detection of hot gaseous halo around giant spiral galaxies such as NGC1961 (Anderson et al. 2011) and UGC12591 (Dai et al. 2012) (see also Mathur et al. 2008). Though the reported masses in warm-hot halos of these galaxies are significant, they are not a major contributor to the galactic missing baryons. It is possible that the reported masses are underestimated because studies based only on emission are biased toward detecting only higher density gas.

Milky Way offers an ideal opportunity to characterize the warm-hot CGM, both in absorption and emission. The UV absorbers provide strong evidence for the presence of the warm gas ( $T < 10^6$  K) through absorption lines of Si IV, C IV (Lehner & Howk 2011) and O VI (Sembach et al. 2003). The hotter phase of the warm-hot gas, at temperatures  $10^6 - 10^7$  K, can again be probed by even more highly ionized metals. Indeed, absorption lines due to O VII and O VIII at redshift zero have been detected in X-rays toward extragalactic sight-lines by *Chandra* and *XMM-Newton* (Fang et al. 2006; Bregman 2007; Williams et al. 2005; Gupta et al. 2012, hereafter Paper-I). The presence of the hot halo observed through  $z = 0$  X-ray absorption lines is generally agreed upon, but its density, path-length, and mass is a matter of debate (Mathur 2012).

In Paper-I, we performed a comprehensive survey of O VII and O VIII absorption lines at  $z = 0$  using *Chandra* observations. We found that the O VII absorption lines along several sightlines are saturated and the implied column densities are larger than in previous studies. We also found a large covering fraction (72%) of the absorbing gas. We used newer and better measurements of the emission measure to solve for the density and the path-length of the absorbing/emitting plasma. With these improvements we found that there is a huge reservoir of ionized gas around the Milky Way, with a mass of  $\geq 6 \times 10^{10} M_{\odot}$  and a radius of over 100 kpc, consistent with theoretical models (Feldmann et al. 2013; Fang et al. 2012). The mass probed by this warm-hot gas is larger than in any other phase of the CGM and is comparable to the entire baryonic mass of the Galactic disk of  $6 \times 10^{10} M_{\odot}$ . The baryonic fraction  $f_b$  of this warm-hot gas varies from 0.09-0.23 depending on the estimates of the virial mass of the Milky Way, from  $10^{12} M_{\odot}$  to  $2.5 \times 10^{12} M_{\odot}$  (Boylan-Kolchin et al. 2013),

bracketing the Universal value of  $f_b = 0.17$ .

Until recently most of the absorption/emission studies of the warm-hot gas in the Milky-way galactic halo assumed an average emission measure (EM) over the sky, and the recent value used in Paper-I is  $EM \sim 0.003 \text{ cm}^{-6} \text{ pc}$ . However, analysis of the RASS data (Snowden et al. 2000) and subsequent shadow observations have shown that there is significant spatial variation in the Galactic halo emission (Gupta et al. 2009, and references therein). A systematic study of the emission measure of the hot gas in the Galactic halo was conducted recently by Yoshino et al. (2009) and Henley et al. (2010) with the *Suzaku* and *XMM-Newton* archival data respectively. They observed that the halo temperature is fairly constant across the sky ( $\approx 1.8 - 2.4 \times 10^6 \text{ K}$ ), whereas the halo emission measure varies by an order of magnitude. This may affect the estimates of density and path-length of the halo warm-hot gas and the subsequent mass measurement.

Instead of the averages of emission and absorption measurements used in previous studies, using emission measures close to absorption sightlines would be a significant step forward for probing the anisotropy of the Galactic CGM. With this goal, we re-examined the emission/absorption measurements in directions of bright quasars Mrk 421 and PKS 2155-304 at redshifts of 0.030 and 0.116, respectively. These extragalactic sources have highest quality *Chandra* and *XMM-Newton* grating spectra, which have been analyzed in detail by several authors (Nicastrò et al. 2002, 2005; Kaastra et al. 2006; Williams et al. 2006, 2007; Fang et al. 2006; Bregman 2007, Paper-I). Both *Chandra* and *XMM-Newton* detected the local ( $z=0$ ) O VII and O VIII absorption lines towards these sightlines with high confidence. In this work, we used the results from Paper-I for absorption measurements, which are in agreement with other works. For the emission measurements we analyzed the *Suzaku* archival data. Hagihara et al. (2010) have published the *Suzaku* data from adjacent fields of PKS 2155-304, but we re-analyze these data for consistency with the Mrk 421 field and also because we use a different method (as described in Henley et al. (2010)) to constrain the Galactic halo emission measure in this direction. The paper is organized as follows: in section 2 we present *Suzaku* observations, detailing the process for extracting the Galactic halo emission measure. In section 3 we present spectral modeling and in section 4 we review absorption measurements from Paper I. In section 5 we present combined absorption/emission analysis and the discussion is in §6. We conclude in §7.

## 2. *Suzaku* Observations and Data Reduction

*Suzaku* observed four X-ray blank sky fields adjacent to PKS 2155-304 and Mrk 421, two in each direction, in June 2008 and November 2009 respectively. Fig. 1 shows the

RASS (0.1-2.4 keV) images in the vicinity of PKS 2155-304 and Mrk 421, along with the *Suzaku* pointing of nearby blank sky fields. The observation IDs, dates, pointing directions and exposure times are summarized in Table 1.

In this work we only used the data from X-ray Imaging Spectrometer (XIS) on board *Suzaku*. For data reduction we followed the procedure described in details in Gupta et al. (2009) and Mitsuishi et al. (2012). The data reduction and analysis were carried out with HEASoft version 6.13 and XSPEC 12.7.0 with AtomDB ver.2.0.1. In addition to standard data processing (e.g.  $ELV > 5$  and  $DYE\ ELV > 20$ ), we performed a data screening with the cut-off-rigidity (COR) of the Earth’s magnetic field, which varies as *Suzaku* traverses its orbit. During times with larger COR values, fewer particles are able to penetrate the satellite and the XIS detectors. We excluded times when the COR was less than 8 GV, which is greater than the default value (COR 4 GV) for all four observations, as lowest possible background was desired.

We produced the redistribution matrix files (RMFs) by *xisrmfgen* ftool, in which the degradation of energy resolution and its position dependence are included. We also prepared ancillary response files (ARFs) using *xissimarfgen* ftool (Ishisaki et al. 2007), which takes into account the spatially varying contamination on the optical blocking filters of XIS sensors which reduce the detector efficiency at low energies (Koyama et al. 2007). For the ARF calculations we assumed a uniform source of radius  $20''$  and used a detector mask which removed the bad pixel regions.

Although reduced by the Earth’s magnetic field, *Suzaku* still has a noticeable particle background. We estimate the total instrumental background from a database of the night Earth data with the *xisnxbgen* ftools task (Tawa et al. 2008). Night Earth data were collected when the telescope was pointed at the night Earth (elevation less than  $-5$  degree, and pointed at night side rather than day). The instrumental background was removed from the event files of the observations. The event files were also carefully screened for telemetry saturation and other artifacts.

Determination of the Galactic halo emission measure is highly complex. Until recently, ROSAT 3/4 keV maps (Snowden et al. 1997) were used for this purpose (e.g. in Bregman et al. 2007), but ROSAT had insufficient spectral resolution to separate the foreground (Local Bubble (LB), plus solar wind charge exchange, (SWCX)) and background (Galactic halo plus extragalactic emission) components. Observations with *XMM-Newton* and *Suzaku* are much better for this purpose, with their large field of view and spectroscopic capabilities. Gupta et al. (2009) and Henley et al. (2010) have discussed in details the process of extracting Galactic halo emission measure, but the complexity of this analysis warrants some discussion here.

For determination of the Galactic halo emission measure, which is such a weak signal, we are required to perform careful analysis with several steps: (1) Determine the contribution from the LB and SWCX. We have taken care to choose data when the variable component of the SWCX is minimum (§2.1). Any residual and non-varying component of the SWCX is determined by modeling the soft X-ray spectrum with an unabsorbed thermal plasma emission model (§3.1). A detailed estimate of the individual SWCX and LB contribution based on solar wind flux and ROSAT All Sky Survey (RASS) data has also been used to verify the accuracy of our approach and the systematics. (2) Determine the contribution from unresolved extragalactic background sources. This is modeled with an absorbed power law (§3.2). (3) Finally determine the hotter Galactic halo contribution, modeled as an equilibrium thermal plasma component absorbed by the gas in the galactic disk (§3.3).

## 2.1. Reducing SWCX component

Diffuse X-ray background at energies below 1 keV is severely affected by SWCX, which varies both in spectral composition and flux on scales of hours to days. The SWCX is produced when highly ionized solar wind particles interact with neutral gas, causing an electron jump from the neutral atom to an excited level in the ion. The electron then cascades to the lower energy level of the ion, emitting soft X-rays and other lines in the process. The neutral atoms may be in the outer reaches of the Earth’s atmosphere (giving rise to geocoronal emission), or they may be in the interstellar material flowing through the solar system (giving rise to heliospheric emission). The minimum SWCX plus LB contribution to O VII line intensities has been estimated to be about 2 Luminosity Units (LU;  $\text{ph s}^{-1} \text{cm}^{-2} \text{sr}^{-1}$ ) (Yoshino et al. 2009; Henley et al. 2013).

As a part of an XMM-Newton “Large Program” we have also conducted a monitoring campaign of the high latitude molecular cloud MBM12 to study the temporal variation of the heliospheric SWCX emission. By choosing a molecular cloud we remove the non-local X-ray background and maximize the SWCX signal. The campaign used 5 different pointings spanning a time of almost 10 years and correlates the oxygen emission with solar wind conditions (Galeazzi et al. 2013). The Suzaku data of Mrk 421 and PKS2155-304 were obtained during a minimum of the Sun’s 11-year cycle, a period that is well characterized by the MBM12 campaign. The data indicate that the heliospheric SWCX contribution to O VII in the MBM12 direction during the Mrk 421 and PKS2155-304 observations was about 1 LU.

While the SWCX contribution was low, it was non-zero and it could be further minimized with proton flux filtering (Smith et al. 2007; Yoshino et al. 2009; Yoshitake et al. 2013). This

is because the geocoronal component of the SWCX depends on the solar wind proton flux incident on the Earth and on the sightline path through the magnetosheath. The higher proton flux indicates higher ion flux that produces a contamination of specific lines through the charge exchange process as described in Ezoe et al. (2010). We obtained the solar wind proton flux data from OMNIWeb<sup>1</sup>. Figures 2 & 3 show the lightcurves of Mrk 421 and PKS 2155-304 off-fields observations and of solar wind proton flux during these exposures. We removed the portions of *Suzaku* observations that were taken when solar wind proton flux exceeded  $4 \times 10^8 \text{ cm}^{-2} \text{ s}^{-1}$ ; this threshold is typically used to reduce the geocoronal SWCX contribution (Mitsuda et al. 2007; Hagihara et al. 2010; Mitsuishi et al. 2012).

Even after applying the above proton flux filtering, the spectrum could be contaminated by geocoronal SWCX, as this threshold is higher than the average proton flux of  $2.8 \times 10^8 \text{ cm}^{-2} \text{ s}^{-1}$  at 1 AU (Henley et al. 2010). However, if we apply tighter constraints on proton flux filter we lose large portions of the *Suzaku* exposure time, so the residual SWCX contribution to the soft X-ray flux is taken into account with spectral modeling (§3.1).

### 3. Spectral Modeling

We cleaned XIS1 spectra extracted from each *Suzaku* observation following the above procedure and then performed spectral modeling. As noted above, the spectra have three distinct components: (1) a foreground component made of residual SWCX and LB; (2) a background component made of unresolved extragalactic sources; and (3) the Galactic halo component. Below we discuss each of these in turn.

#### 3.1. Shape and normalization of the foreground component.

We model the foreground as an unabsorbed plasma in collisional ionization equilibrium (CIE) with thermal emission. The parameters of this model are plasma temperature and normalization. We fixed the temperature  $T = 1.2 \times 10^6 \text{ K}$  as suggested by data from RASS (Snowden et al. 1998, 2000; Kuntz & Snowden 2000) and further supported by current X-ray shadow observations (for summary see Gupta et al. 2009).

To determine the normalization we used Snowden et al. (2000) catalog of SXR shadows, consisting of 378 shadows in the RASS. This catalog contains the foreground and background R12 (1/4 keV) count-rates. Following Henley et al. (2010), we found 5 shadows

---

<sup>1</sup> (<http://omniweb.gsfc.nasa.gov/>)

in the catalog closest to our sightlines, and averaged their foreground count-rates, weighted by the inverse of their distances from the *Suzaku* sightlines:

$$\text{Foreground R12 countrate} = \frac{\sum R_i/\theta_i}{\sum 1/\theta_i} \quad (1)$$

where  $R_i$  is the foreground R12 count-rate for the  $i$ th shadow, and  $\theta_i$  is the angle between the center of the  $i$ th shadow and the *Suzaku* sightline. Since foreground intensity varies fairly mildly over the sky (Snowden et al. 2000), this method provides a reasonable estimate of the foreground intensity at high latitudes ( $l > 30$  deg) in the R12 band. Then we extrapolated the foreground spectrum from the R12 band to the 0.5 – 1.0 keV soft X-ray band.

In the adjacent fields of Mrk 421 and PKS 2155-304, we calculated the average foreground R12 count-rate of  $(767 \pm 243) \times 10^{-6}$  counts s<sup>-1</sup> arcmin<sup>-2</sup> and  $(397 \pm 143) \times 10^{-6}$  counts s<sup>-1</sup> arcmin<sup>-2</sup> respectively. Using the above calculated count-rate, we determine the normalization of the foreground thermal component assuming  $T = 1.2 \times 10^6$  K.

### 3.2. Background component.

The background component from unresolved extragalactic sources was modeled with an absorbed power law. The parameters of the model are the Galactic column density, which was held fixed, and power-law slope and normalization, which were left as free parameters in the spectral fit; the results are given in Table 2. We point out that the power law component is the dominant contributor to the spectrum above 1.5 keV, but does not dominate at softer energies where the Galactic halo component is present.

### 3.3. Galactic halo component.

The Galactic halo emission was modeled as an equilibrium thermal plasma component absorbed by the cold gas in the Galactic disk. The parameters of this model are the plasma temperature, normalization, and the Galactic column density. For the absorption, we used the XSPEC *wabs* model, which uses cross-sections from Wisconsin (Morrison & McCammon 1983) and uses the Anders & Ebihara (1989) relative abundances; the column density along our sightlines was fixed to the observed values (Dickey & Lockman 1990). For plasma thermal emission, we used the Astrophysical Plasma Emission Code (*APEC*: Smith & Cox 2001) and the temperature and normalization were left as free parameters of the fit.



Finally, *Suzaku* spectra of Mrk 421 and PKS 2155-304 off-fields were fitted using all the three components noted above. We measured the galactic halo temperature of  $\log T = (6.31 \pm 0.04) \& (6.32 \pm 0.02)$  K and emission measure of  $(2.4 \pm 0.5) \times 10^{-3} \& (2.6 \pm 0.4) \times 10^{-3} \text{ cm}^{-6} \text{ pc}$  near Mrk 421 off-field 1 and off-field 2 respectively.

The galactic halo emission measure and temperature near PKS 2155-304 off-field 1 and off-field 2 are  $(4.0 \pm 0.5) \times 10^{-3} \& (4.3 \pm 0.4) \times 10^{-3} \text{ cm}^{-6} \text{ pc}$  and  $\log T = (6.37 \pm 0.02) \& (6.35 \pm 0.02)$  K respectively.

The temperature and emission measure of Galactic halo thermal component were consistent between the two fields near PKS 2155-304 and Mrk 421 sightlines. Thus to obtain better constraints we fitted the above mentioned models simultaneously to both the off-field spectra with a single set of parameters (except for the power-law) in each direction. The fits are shown in Fig. 4, and the model parameters are presented in Table 2.

### 3.3.1. Additional contamination due to SWCX.

From each spectrum, we also evaluated line centers and surface brightness of O VII  $K\alpha$  and O VIII  $K\alpha$  emission lines. In the best fit model of each observation, we replaced the *APEC* model with *VAPeC* model for the Galactic halo component, whose oxygen abundance was set to 0 and added two Gaussian lines for O VII  $K\alpha$  and O VIII  $K\alpha$  emission. The abundances of other elements were fixed to be 1 solar, and temperatures of *VAPeC* components were fixed to the best-fit values for the individual fits. The line centers and the surface brightnesses were derived from these spectral fits.

The O VII intensities estimated from spectral fitting were consistent within 1 sigma error between Mrk 421 off-field 1 and off-field 2 observations (Table 3). The PKS 2155-304 off-field 1 and off-field 2 intensities, however, were different,  $7.4 \pm 0.7 \text{ ph s}^{-1} \text{ cm}^{-2} \text{ sr}^{-1}$  (LU) and  $8.3 \pm 0.7 \text{ LU}$  respectively. We investigated whether this difference is due to contamination from geocoronal SWCX as follows. While during the Mrk 421 pointings the solar wind proton flux was consistently below  $2.8 \times 10^8 \text{ cm}^{-2} \text{ s}^{-1}$ , during the PKS 2155-304 off-field 1 observation, the proton flux varied considerably from less than about  $2.0 \times 10^8 \text{ cm}^{-2} \text{ s}^{-1}$  to about  $4.0 \times 10^8 \text{ cm}^{-2} \text{ s}^{-1}$  (figure 4). We extracted and modeled the spectra during these intervals and found that the O VII intensity changed from  $5.3 \pm 1.2$  to  $7.8 \pm 1.1 \text{ LU}$ . During the PKS 2155-304 off-field 2 observation the proton flux was always higher than  $2.0 \times 10^8 \text{ cm}^{-2} \text{ s}^{-1}$  and the O VII intensity remained on higher side at  $8.3 \pm 0.7 \text{ LU}$ . Considering the observational geometry for our pointings, we expect the contribution from geocoronal SWCX to the O VII line to be negligible for proton fluxes below  $2.0 \times 10^8 \text{ cm}^{-2} \text{ s}^{-1}$ . This is not

true, however, for the higher flux encountered during the PKS 2155-304 pointings. Based on the numbers reported above, we estimate that the contamination due to geocoronal SWCX is of the order of  $\sim 2$  LU. We therefor added this SWCX contribution to the normalization of the foreground component and fitted the PKS 2155-304 off-field spectra again. The parameters in Table 2 refer to this final fit.

### 3.4. Systematic error on Emission measurement

In our spectral model we fixed the temperature and normalization of the foreground component, otherwise there would be degeneracy between the foreground and Galactic halo intensities. This results in systematic errors on Galactic halo emission measure due to our assumed spectrum of the foreground component. We have fixed the foreground normalization by extrapolating the foreground spectrum from the R12 (0.1 – 0.284 keV) band into the *Suzaku* 0.5 – 1.0 keV band. However, this extrapolation may not be a correct estimate of the foreground normalization, because the spectral shapes in the two bands may be different. Additionally, relative contributions of LB and SWCX emission are likely to differ in these bands (Koutroumpa et al. 2009a,b).

A conservative way to estimate the systematic error is to determine the upper limit on the galactic halo emission measure. To do that, we estimated the lower limit on the combined emission of LB plus heliospheric SWCX (the contribution from geocoronal SWCX has already been discussed in details on section 3.3.1). As our observations were performed during a time of low solar wind activity, a conservative estimate is to assume that the minimum heliospheric SWCX contribution is zero. For the lower limit on LB emission, we followed the procedure in Lallement (2004). We found that the lower limit on the foreground emission is  $0.0029 \pm 0.0004 \text{ cm}^{-6}\text{pc}$  resulting in the upper limit on Galactic halo emission of  $0.0003 \pm 0.0005 \text{ cm}^{-6}\text{pc}$  and  $0.0051 \pm 0.0004 \text{ cm}^{-6}\text{pc}$  in the directions of Mrk 421 and PKS 2155 – 304 respectively. Thus we estimate the systematic errors on the emission measure to be  $0.0005 \text{ cm}^{-6} \text{ pc}$  and  $0.0009 \text{ cm}^{-6} \text{ pc}$  for the two directions.

We also used a method described in Henley et al. to estimate the systematic errors by reanalyzing each spectrum, using the median foreground R12 intensity ( $600 \times 10^{-6} \text{ counts s}^{-1} \text{ arcmin}^{-2}$ ) to fix the foreground normalization instead of that from the 5 nearby shadows (§3.1). The systematic errors we get using this method are  $0.0004 \text{ cm}^{-6} \text{ pc}$  and  $0.0005 \text{ cm}^{-6} \text{ pc}$  for the two directions. These are lower than our previous estimates, so to be conservative we adopted errors estimated above. Note that if the Galactic halo emission measure is systematically lower, then the implied pathlength is higher, and the mass of the CGM would also be higher (see Gupta et al. 2012, Mathur 2012).

#### 4. *Chandra* Absorption Measurements

In Paper-I, we measured the equivalent widths (EWs) of  $z = 0$  O VII  $K\alpha$  absorption line of  $11.6 \pm 1.6$  mÅ and  $9.4 \pm 1.1$  mÅ towards PKS 2155-304 and Mrk 421 respectively. We also detected the  $z = 0$  O VII  $K\beta$  absorption toward both sight-lines with EWs of  $4.2 \pm 1.3$  mÅ and  $4.6 \pm 0.7$  mÅ respectively. The observed  $\frac{EW(O_{VII} K\beta)}{EW(O_{VII} K\alpha)}$  ratio of  $0.36 \pm 0.12$  and  $0.49 \pm 0.09$  (in comparison to expected ratio of 0.156), clearly shows that O VII  $K\alpha$  lines are saturated. Thus using the “curve-of-growth” analysis we constrained the O VII column densities of  $\log(N_{O_{VII}}) = 16.09 \pm 0.19$  and  $16.22 \pm 0.23$  cm<sup>-2</sup> towards PKS 2155-304 and Mrk 421 respectively. For detailed analysis of absorption measurements, we refer the readers to Paper-I.

In Paper-I we also reported on the  $z = 0$  O VIII absorption lines in the spectra of Mrk 421 and PKS2155-304. With column density ratio of O VII to O VIII, we constrained the temperature of the absorbing gas in these sightlines to  $\log T = 6.16 \pm 0.08$  K and  $\log T = 6.27 \pm 0.05$  K respectively. These estimates are comparable to the temperature obtained from galactic halo emission model (Table 2). Given that O VII absorption and emission trace warm-hot gas at similar temperatures, it is reasonable to assume that they arise in the same gas (but see §6.2 and §6.3 where we relax this assumption). We can then combine these two diagnostics to derive physical properties of the warm-hot gas.

#### 5. Combined Emission/Absorption Analysis

The absorption lines measure the column density of gas  $N_H = \mu n_e L$ , where  $\mu$  is the mean molecular weight  $\approx 0.8$ ,  $n_e$  is the electron density and  $L$  is the path-length. The emission measure, on the other hand, is sensitive to the square of the number density of the gas ( $EM = n_e^2 L$ , assuming a constant density plasma). Therefore a combination of absorption and emission measurements naturally provides constraints on the density and the path-length of the absorbing/emitting plasma.

##### 5.1. Mrk 421

The CGM O VII column density towards Mrk 421 is  $16.22 \pm 0.23$  cm<sup>-2</sup> and the average emission measure of two fields 30' away on opposite sides of the Mrk 421 sightline is  $0.0025 \pm 0.0003 \pm 0.0005$  cm<sup>-6</sup> pc. Combining absorption and emission measurements, we solve for the electron density and path-length of O VII emitting/absorbing plasma, following the procedure in Paper-I. Towards the sight-line of Mrk 421 the electron density is given by:

$$n_e = (1.6_{-0.8}^{+2.6} \times 10^{-4}) \left(\frac{0.5}{f_{OVII}}\right)^{-1} cm^{-3} \quad (2)$$

and the pathlength is:

$$L = (334_{-274}^{+685}) \left(\frac{8.51 \times 10^{-4}}{(A_O/A_H)}\right) \left(\frac{0.5}{f_{OVII}}\right)^2 \left(\frac{0.3Z_\odot}{Z}\right) kpc \quad (3)$$

where the solar oxygen abundance of  $A_O/A_H = 8.51 \times 10^{-4}$  is from Anders & Ebihara (1989),  $f_{OVII}$  is the ionization fraction of O VII, and  $Z = 0.3Z_\odot$  is the metallicity.

## 5.2. PKS 2155-304

Toward the sight-line of PKS 2155-304, the halo O VII column is  $16.09 \pm 0.19 cm^{-2}$  and the emission measure is  $0.0042 \pm 0.0003 \pm 0.0007 cm^{-6} pc$ . Combining absorption and emission, we determine the electron density of

$$n_e = (3.6_{-1.8}^{+4.5} \times 10^{-4}) \left(\frac{0.5}{f_{OVII}}\right)^{-1} cm^{-3} \quad (4)$$

and the pathlength of:

$$L = (109_{-82}^{+200}) \left(\frac{8.51 \times 10^{-4}}{(A_O/A_H)}\right) \left(\frac{0.5}{f_{OVII}}\right)^2 \left(\frac{0.3Z_\odot}{Z}\right) kpc \quad (5)$$

We note that the large error bars on the gas density and path-length are dominated by systematic uncertainties in the O VII column density measurements due to line saturation. These error bars do not represent the statistical limit of the measurement. The O VII absorption line EWs and galactic halo emission measure are determined with more than  $5\sigma$  significance.

## 6. Discussion

### 6.1. Comparison with Paper-I

In Paper-I we measured the average O VII column density of  $\log N(O_{VII}) = 16.19 \pm 0.08 cm^{-2}$ . In Mrk 421 and PKS 2155-304 sightlines the measured O VII column densities

are  $\log N_{OVII} = 16.22 \pm 0.23$  &  $16.09 \pm 0.19$   $\text{cm}^{-2}$ , respectively. The best fit value toward Mrk 421 is somewhat larger than the average and that toward PKS 2155-304 is somewhat smaller than the average (Fig. 5), but they are consistent with the average and with each other, within errors.

In Paper-I we also assumed the average emission measure of  $0.0030 \pm 0.0006$   $\text{cm}^{-6}$  pc. The emission measures towards Mrk 421 and PKS 2155-304 of  $0.0025 \pm 0.0006$  &  $0.0042 \pm 0.0008$   $\text{cm}^{-6}$  pc respectively, are significantly different from each other (Fig 5).

Thus in the two sightlines that we consider, the observed column densities are similar, but observed emission measures are different, so their densities and pathlengths must be different. This is because the gas density and path-length are proportional to  $\frac{EM}{N_{OVII}}$  and  $\frac{N_{OVII}^2}{EM}$  respectively. Thus in the direction toward Mrk 421, lower emission measure brings the gas density lower while path-length higher than average. The opposite is true for the PKS2155-304 direction.

Towards Mrk 421 we calculated the density and the path-length of warm-hot gas of  $1.6_{-0.8}^{+2.6} \times 10^{-4}$   $\text{cm}^{-3}$  and  $334_{-274}^{+685}$  kpc respectively. On the other hand, near PKS2155-304 sight-line, we measured the gas density of  $3.6_{-1.8}^{+4.5} \times 10^{-4}$   $\text{cm}^{-3}$  and path-length of  $109_{-82}^{+200}$  kpc. Thus the density and pathlength in the two directions are similar within (large) errors.

This investigation on comparing absorption and emission measurements from adjacent fields provides suggestive evidence that the warm-hot gas in the CGM of the Milky Way is not distributed uniformly. However, the formal errors on derived parameters are too large to make such a claim. We need to perform similar studies for a number of sight-lines to probe the anisotropy of the MW CGM. The mean density and path-length from these two sightlines, of  $\sim 2.6 \times 10^{-4}$   $\text{cm}^{-3}$  and  $\sim 221$  kpc, are consistent with the average from the entire *Chandra* sample (Paper-I), so the mass measurement is unlikely to be very different.

## 6.2. Galactic disk contribution to observed absorption/ emission?

Our interest is to determine the physical properties of the warm-hot gas in the Galactic halo. For this purpose, in Paper-I we chose our targets to be of high Galactic latitude  $|b| \gtrsim 20^\circ$ . The two targets in this paper, Mrk 421 and PKS2155 – 304 have  $b = 65.03$  and  $b = -52.245$  degrees respectively, so the observed O VII absorption should have minimal contribution from the Galactic thick disk. In order to investigate further whether the observed O VII absorption is dominated by the disk of the Galaxy, we looked for the dependence on the observed O VII equivalent width (EW) on  $\sin(|b|)$ ; we expect a clear anticorrelation between these two parameters if the absorption is dominated by the disk. In figure 6 we have plotted EW

vs.  $\sin(|b|)$  for all 21 sightlines in Paper I in which O VII absorption was detected. We see that the data do not show significant anticorrelation (Spearman rank correlation coefficient  $\rho = -0.24$ , with the chance probability of 0.14).

The real anticorrelation we expect, however, is between  $\sin(|b|)$  and column density, not with EW, but we do not have column density measurements for all the 21 sightlines. Given that saturation effects are important in cases of high column densities, there may be crowding at high EW values. Therefore, if the disk contribution is significant we should find that the distribution of EWs is different in low- and high- values of  $\sin(|b|)$ . We tested this using the Student’s t-test and found that  $t = 0.937$ , with the probability that the differences are due to chance = 0.361. Thus once again we do not see any significant differences with  $\sin(|b|)$ . This suggests that the Galactic disk does not contribute significantly to the observed O VII absorption.

Henley & Shelton (2013) also came to the same conclusion for emission measure. They studied 110 *XMM-Newton* sightlines and detected emission from the million degree gas in about 80% of them. They find that the high latitude sky has a patchy distribution of warm-hot gas, but they find no evidence for the observed emission measure to decrease with increasing Galactic latitude (see their figure 5). Therefore they argue that the emitting plasma does not have a disk-like geometry.

Thus, both absorption and emission measurements show no evidence for a significant disk contribution. Nonetheless, if there is *any* contribution from the disk, it would end up strengthening our result in that it would make the inferred halo path-length larger and so the mass; this is explained in detail below.

### 6.3. Assumption of a constant density profile.

In deriving the Galactic halo pathlength and density, we have assumed the density to be constant, as we did in Paper I. A realistic halo is likely to have some density profile that falls with radius, so it is imperative to investigate how reasonable our assumption is and what are the effects of our assumption on our results. This is particularly important because the EM is biased toward high density plasma, while the absorption is sensitive to integrated density.

The observations of other galaxies support the assumption of an extended density profile. As noted in §1, Williams et al. (2013) investigated intervening X-ray absorption line systems toward H2356 – 309 observed by Buote et al. (2009), Fang et al. (2010) and Zappacosta et al. (2010). They found that three of the four absorption systems originate within virial radii

of nearby galaxies or groups with projected distances of 100s of kpc. These observations give evidence for extended warm-hot halos around other galaxies. The  $z = 0.030$  system in Williams et al. is particularly relevant for the present discussion because the observed sightline passes through the halo of a nearby galaxy. The observed column density of this absorption system is  $\log N_{O\text{VII}} = 16.8_{-0.9}^{+1.3}$  at an impact parameter of  $D = 90$  kpc from a nearby galaxy with virial radius of  $R = 160$  kpc. The path-length of the absorber is then  $2\sqrt{R^2 - D^2} = 264.6$  kpc. From the path-length and the column density we calculate the density  $= 7.4 \times 10^{-4} \text{ cm}^{-3}$  (for O VII ionization fraction and metallicity as in Paper-I). This shows that such a high density, even more than what we calculated for the MW halo, is present out to about a hundred kpc from another galaxy as well. This not only shows a MW-type halo around another galaxy, it also shows that the assumption of a flat density profile is reasonable. There is also another circumstantial evidence that the Milky Way warm-hot halo has an extended gas profile. Grcevich & Putman (2009) explain the non-detection of HI in most dwarf spheroidal galaxies near the Milky Way by ram pressure stripping by low density ( $\sim 10^{-4} \text{ cm}^{-3}$ ) hot gas extended out to  $\geq 70$  kpc. This again suggests that our assumption of a single temperature, constant density, extended plasma is reasonable (see also Mathur 2012).

Some authors have used different models to describe density gradients such as a simple exponential profile or a  $\beta$ -model (e.g. Mathur et al. 2008 and references therein). In the simulations of Feldmann et al. (2013), the density is roughly constant above the Galactic disk out to about 100 kpc. Fang et al. (2012) considered a hot halo that is distributed as adiabatic gas with a polytropic index of 5/3, in hydrostatic equilibrium within the Milky Way's dark matter halo with NFW profile (Navarro, Frenk, & White 1997). They also consider a thick disk profile and a cuspy NFW profile and compare these models with the observations of dwarf satellite galaxies (Grcevich & Putman 2009). They find that a Maller & Bullock type flat, extended profile of the hot gas is preferred (see their figure 1). While this is not exactly a constant density profile, it is flat enough that constant density is a reasonable approximation.

Thus observations of external galaxies as well as theoretical models support a reasonably flat and extended (over 100 kpc) density distribution and rule out thick-disk type profile for the hot halo gas. Nonetheless, let us investigate the effect of a density gradient on our results. Combining the information of EM with absorption column density we measure the density and pathlength of the absorbing/ emitting plasma, assuming a single density. Therefore we have density  $n \propto EM/N_H$  and so the path-length  $L \propto N_H^2/EM$ . Now let us say that the density is actually not constant, but has a high density component  $n(\text{High})$  and a low density component  $n(\text{Low})$  such that  $n(\text{High}) \gg n \gg n(\text{Low})$ . We are considering just two components here for simplicity, but the argument can be generalized to many components or

to any density profile. The observed EM is then a sum of the EM from the two components:  $EM = n(High)^2 L(High) + n(Low)^2 L(Low)$  where  $L(High)$  and  $L(Low)$  are the pathlengths of the high and low density components respectively. Similarly, the observed column density  $N_H = n(High)L(High) + n(Low)L(Low)$  (ignoring constants). To satisfy these constraints,  $n(High) \gg n \gg n(Low)$  necessarily implies that  $L(High) \ll L \ll L(Low)$ . Thus the path-length of the low density component  $L(Low)$  is necessarily larger than the pathlength calculated assuming a single density. Given that the implied mass goes as  $L^3$ , the mass also becomes more than that calculated assuming a single density. Thus we see that *any* density gradient would make the Galactic halo more extended and more massive than what we find under a single density assumption. And this is true for any contribution from denser components such as a thick disk or from clumping. This conclusion is mathematically robust and can be generalized to any density gradient. Since this argument may not be obvious, we have discussed it further in the Appendix.

## 6.4. Comparison with other works

### 6.4.1. PKS2155 – 304

Hagihara et al. (2010) have compared the O VII absorption with the galactic halo emission in the adjacent field of PKS2155-304. They measured the O VII column density of  $15.76_{-0.12}^{+0.09} \text{ cm}^{-22}$ , which is smaller than our measured value of  $16.09 \pm 0.19 \text{ cm}^{-2}$ . They measured the O VII equivalent width of  $13.3 \pm 2.8 \text{ m\AA}$  and the Doppler parameter  $b$  of  $294_{-220}^{+149} \text{ km s}^{-1}$ . Though their measured equivalent width is consistent with our measurement, the Doppler parameter  $b$  is much larger than our  $1\sigma$  constraints of  $35 - 94 \text{ km s}^{-1}$ . Due to larger Doppler parameter they underestimate the O VII column density by a factor  $\approx 2$ . For the gas at temperature of about  $2 \times 10^6 \text{ K}$ , the velocity dispersion parameter  $b$  should be of the order of  $45 \text{ km s}^{-1}$ , consistent with our measurement. While there could be additional contribution to the line width due to microturbulence,  $294 \text{ km s}^{-1}$  appears to be excessively high.

Hagihara et al. estimated the lower and upper limits on galactic halo emission measure of  $2.0 \times 10^{-3}$  and  $4.9 \times 10^{-3} \text{ cm}^{-6} \text{ pc}$ , assuming 3.5 LU for the foreground O VII emission and zero normalization of foreground component, respectively. Our measured value of  $0.0042 \pm 0.0006 \text{ cm}^{-6} \text{ pc}$  is within this range.

Combining the absorption and emission measurements they determined the halo path-

---

<sup>2</sup>The reported errors from Hagihara et al. are at 90% confidence level



length and density of  $4.0_{-1.4}^{+1.9}$  kpc and  $(7.7_{-1.7}^{+2.3}) \times 10^{-4}$   $\text{cm}^{-3}$  respectively, assuming solar metallicity and O VII ionic fraction of 1. Hagihara et al. upper limit on galactic halo path-length of 5.4 kpc is in contradiction with our measurement of  $L > 30$  kpc. This discrepancy is due to (a) O VII column density (their column is  $\sim 2$  times smaller than ours), (b) oxygen abundance ( $Z_{\odot}$  versus  $0.3Z_{\odot}$ ), and (c)  $f_{\text{OVII}}$  of 1 versus 0.5.

Cosmological simulations (Toft et al. 2002; Sommer-Larsen 2006) of formation and evolution of disk galaxies show that outside the galactic disk the mean metallicity of gas is  $Z = 0.2 \pm 0.1Z_{\odot}$ . These values of metallicities are also consistent with observational results for the spiral galaxy NGC 891 (Hodges-Kluck & Bregman 2013), the outskirts of groups (Rasmussen et al. 2009) and clusters of galaxies (e.g., Tamura et al. 2004). Thus it is highly unlikely that outside the galactic disk metallicity is as high as solar. The lower value of O VII column density and higher metallicity used by Hagihara et al. underestimate the path-length by a factor of  $\sim 13$ . The difference in  $f_{\text{OVII}}$  would further add a factor of four (see Paper-I for justification of  $f_{\text{OVII}} = 0.5$ ).

The other major difference between our analysis and Hagihara et al. is of assumption of gas density distribution. Hagihara et al. favor the exponential disk model in which temperature and density of the hot gas falls off exponentially along the vertical direction. Such a profile is based on Yao et al. (2007, 2009), required to account for the fact that they measured different halo temperatures from emission and absorption analysis. We do not have this requirement; we found similar temperature for the Galactic halo from both absorption and emission analysis. In any case, see §6.3 above.

#### 6.4.2. Mrk 421

Sakai et al. (2012) combine the absorption and emission measurements towards Mrk 421 and measured the galactic halo path-length and density of  $1.6_{-0.9}^{+3.6}$  kpc and  $(1.5_{-0.5}^{+0.7}) \times 10^{-4}$   $\text{cm}^{-3}$  respectively. The reported path-length again is in contradiction with our measurements. Since this is a conference proceeding paper, we do not have detailed information about their analysis.

#### 6.4.3. Henley & Shelton 2013

Recently Henley & Shelton (2013) published new results on the galactic halo emission measure towards 110 *XMM-Newton* sightlines. They found galactic halo temperature is fairly uniform (median =  $2.22 \times 10^6$  K), consistent with their previous analysis (Henley et al.

2010). However their current estimates on galactic halo emission measure are systematically lower, with median value of  $1.9 \times 10^{-3} \text{ cm}^{-6}\text{pc}$  compared to  $3.0 \times 10^{-3} \text{ cm}^{-6}\text{pc}$  from the previous paper. As the gas density and path-length of galactic halo are proportional to  $\frac{EM}{N_{OVII}}$  and  $\frac{N_{OVII}^2}{EM}$  respectively (§6.1), the lower emission measure increases the path-length and decreases the density by a factor of  $\sim 1.6$  from the Paper-I values. Thus mean path-length and mass of the hot gas in CGM of the Milky-way becomes  $L = 382 \pm 160 \text{ kpc}$  and  $M_{total} = (5.9 \pm 5.4) \times 10^{11} M_{\odot}$  (for  $Z = 0.3Z_{\odot}$ ), respectively, compared to  $L = 239 \pm 100 \text{ kpc}$  and  $M_{total} = (2.3 \pm 2.1) \times 10^{11} M_{\odot}$  in Paper I. Thus, if this new value of the average emission measure is correct, most of the Galactic missing baryons would be accounted for by the warm-hot halo.

## 7. Conclusions

In paper-I we compared average absorption and emission measurements of the warm-hot gas in the CGM to derive its average physical properties such as density, pathlength and mass. The absorption column density as well as the emission measure vary considerably across the sky, so it is far more appropriate to determine emission measures close to absorption sightlines and derive physical properties along each sightline independently. In this paper we expand on the previous work by comparing absorption and emission along two sightlines: toward Mrk 421 and PKS2155-304. We present *Suzaku* observations of fields close to these sightlines. We find that along the Mrk 421 direction, the emission measure is lower than the average, while the opposite is true in the PKS2155-304 sightline. The mean values from these two sightlines are consistent with the average, so the mass of the CGM is unlikely to be very different from that in Paper-I (but see §6.4.3).

In the two sightlines we consider, the observed column densities are similar, but observed emission measures are different, so their densities and pathlengths must be different. This provides a suggestive evidence that the warm-hot gas in the CGM of the Milky Way is not distributed uniformly, but the formal errors on derived parameters are too large to make such a claim. In future studies we will explore the entire distributions of column densities and emission measures (fig. 6) for combined absorption and emission analysis along multiple sightlines. Large fields of view and spectroscopic capabilities of *XMM-Newton* and *Suzaku* are ideal for determining emission measures close to bright AGN sightlines, which are used for absorption measurements. With more such studies, we will be able to better characterize the CGM anisotropy and measure its mass more accurately. Moreover, we can then compare the observational results with theoretical models (§6.3) and investigate if/how the CGM structure is related to the larger scale environment of the Milky Way.

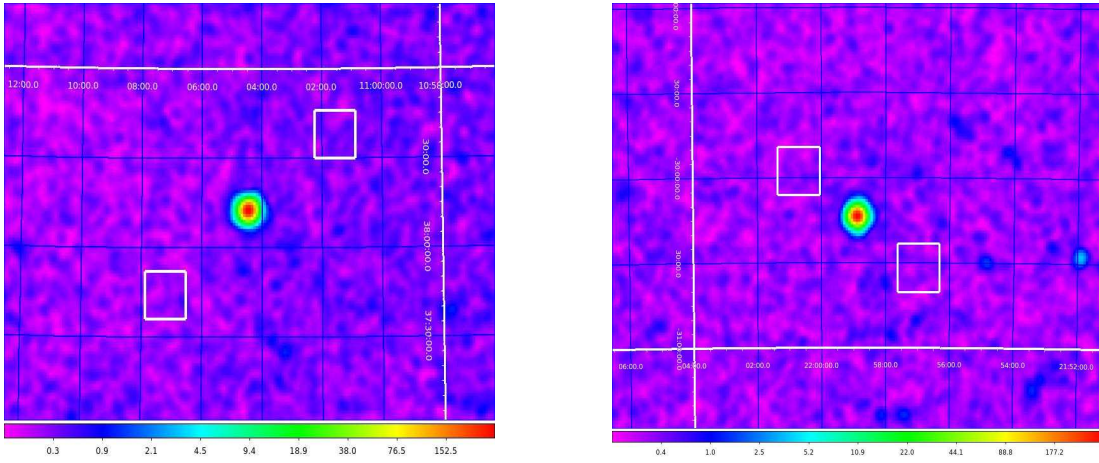


Fig. 1.— RASS map ( $4 \text{ deg} \times 4 \text{ deg}$ ) in the vicinity of Mrk 421 (*left*) and PKS 2155-304 (*Right*). The white squares show the Suzaku pointings used in this investigation, separated by  $\sim 1.4 \text{ deg}$  and  $\sim 1.0 \text{ deg}$  in case of Mrk 421 and PKS2155-304, respectively. The gray scale represent the log of ROSAT broad band counts per pixel.

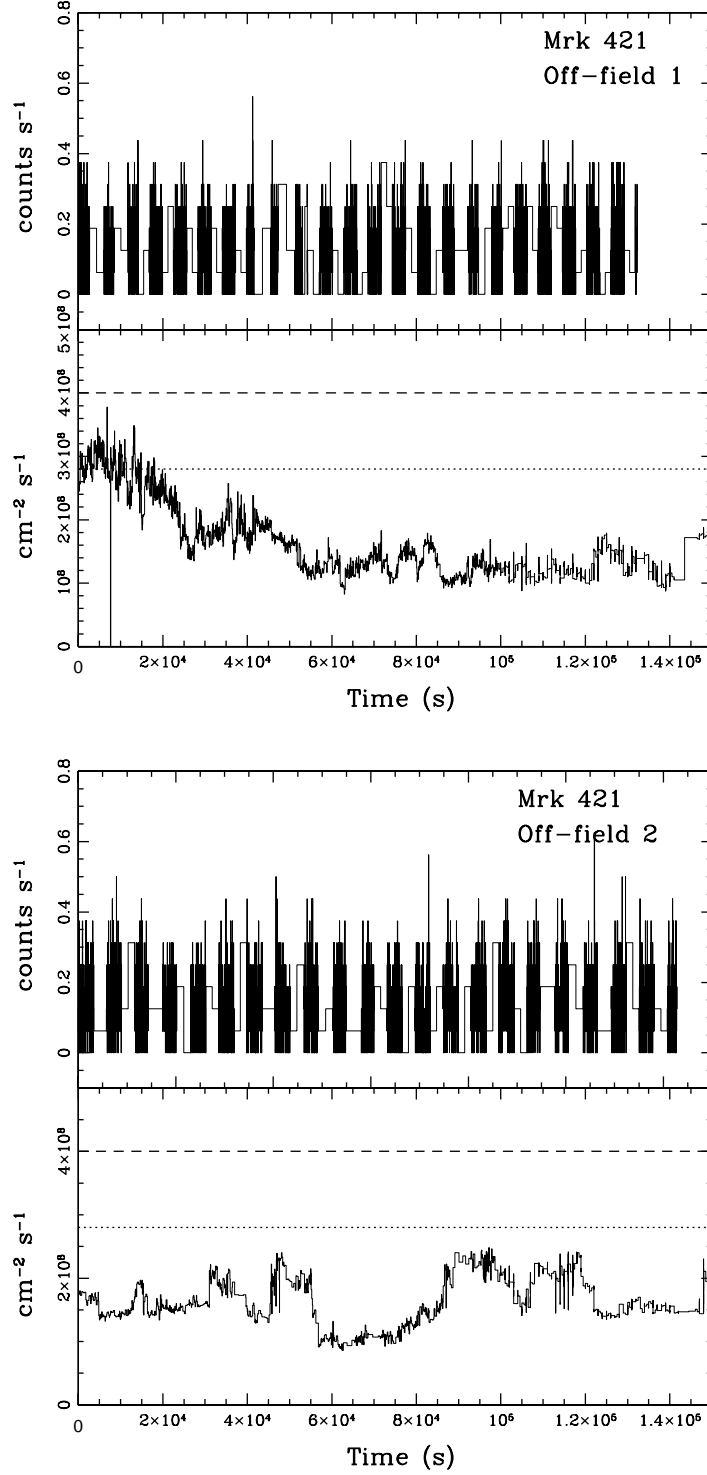


Fig. 2.— XIS1 0.5-2.0 keV light curve (*upper panel*) and solar wind proton flux data from OMNIWeb (*lower panel*) in Mrk 421 Off-field1 (top) and Off-field2 (bottom) observation periods. The *dashed* and *dotted* lines show the proton flux threshold level ( $4 \times 10^8 cm^{-2} s^{-1}$ ) used in this investigation and the average proton flux at 1 AU ( $2.8 \times 10^8 cm^{-2} s^{-1}$ ) respectively.

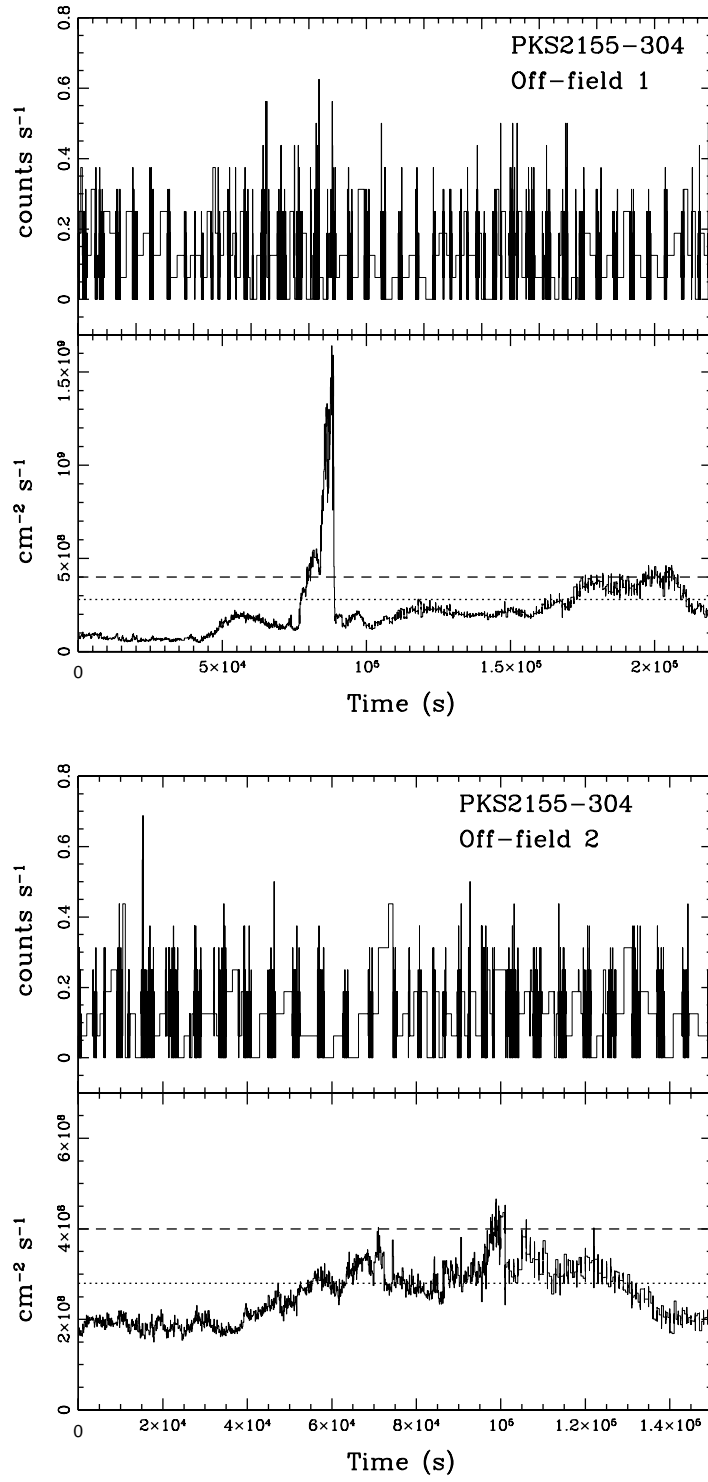


Fig. 3.— Same as fig. 3 for PKS 2155-304.

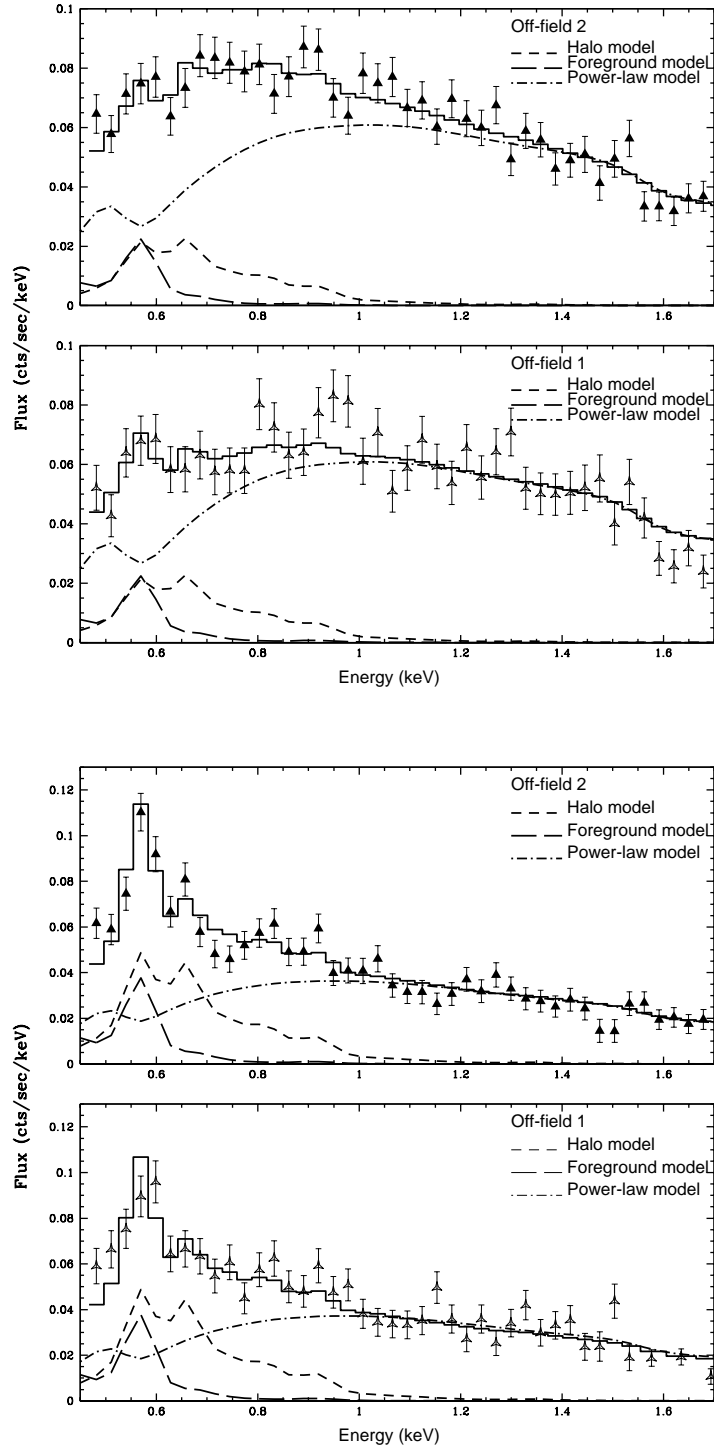


Fig. 4.— Simultaneous fits to Off-field 1 and Off-field 2 Suzaku spectra of regions near Mrk 421(*top*) and PKS2155-304(*bottom*). The dashed curves represent the galactic halo emission model.

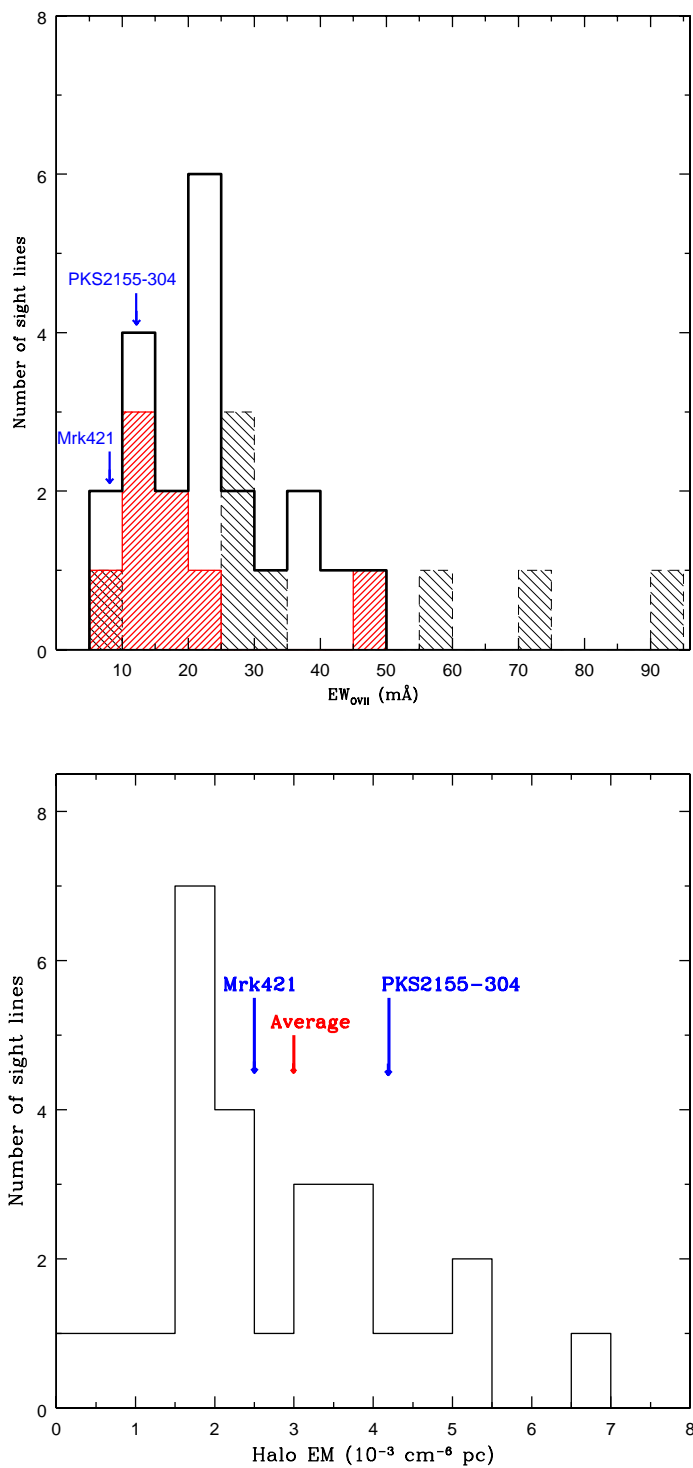


Fig. 5.— *Top*: Distribution of O VII  $K\alpha$  line EW for the parent sample (Paper-I). The red shaded region corresponds to the sub-sample used in Paper-I. *Bottom*: Distribution of galactic halo emission measure using data from Henley et al. (2010). The vertical arrows mark the O VII  $K\alpha$  EW and emission measure towards Mrk 421 and PKS2155-304.

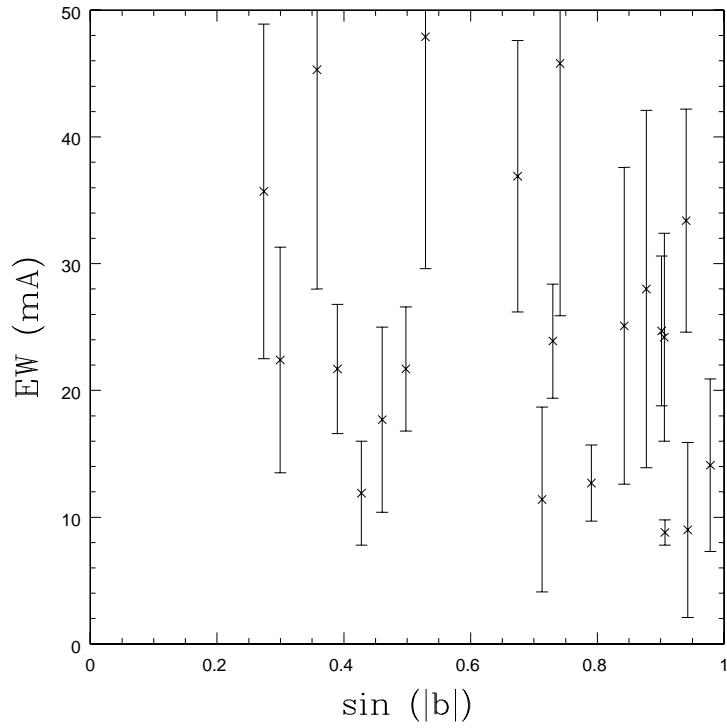


Fig. 6.— Equivalent widths of O VII absorption lines are plotted vs.  $\sin(|b|)$  where  $b$  is the Galactic latitude of the sightline. The data are from Paper-I (their figure 3). We see no anticorrelation between EW and  $\sin(|b|)$ ; this implies that the Galactic thick disk does not contribute significantly to the observed strengths of absorption lines.



Table 1. Details of our Suzaku observations.

Target	Observation ID	Start Time UT	End Time UT	Exposure <sup>a</sup> ks
<b>Mrk421-off-field1</b>	503082010	2008-04-29 18:32:39	2008-05-02 08:30:08	48
<b>Mrk421-off-field2</b>	503083010	2008-05-02 08:31:41	2008-05-04 17:30:19	50
<b>PKS2155-off-field1</b>	504086010	2009-11-09 01:34:20	2009-11-10 19:25:07	45
<b>PKS2155-off-field2</b>	504087010	2009-11-11 10:45:08	2009-11-13 07:37:24	72

<sup>a</sup>Good-Time-Interval after removing the exposure affected by high proton flux.

Table 2. Model parameters of the spectral fits

Dataset(s)	Local component <sup>a</sup>		Galactic Halo		Power Law		$\chi^2/dof$
	$\log T$ K	E.M. <sup>b</sup> $10^{-3} \text{ cm}^{-6} \text{ pc}$	$\log T$ K	E.M. $10^{-3} \text{ cm}^{-6} \text{ pc}$	$\Gamma^c$	Norm <sup>d</sup>	
<b>Mrk 421</b>	6.08	7.3	$6.32 \pm 0.03$	$2.5 \pm 0.6$			289/244
Off-field 1					$1.54 \pm 0.04$	$17.3 \pm 0.6$	
Off-field 2					$1.76 \pm 0.04$	$18.3 \pm 0.5$	
<b>PKS2155-304</b>	6.08	9.7	$6.36 \pm 0.02$	$4.2 \pm 0.8$			313/281
Off-field 1					$1.60 \pm 0.05$	$9.3 \pm 0.3$	
Off-field 2					$1.65 \pm 0.04$	$9.5 \pm 0.3$	

<sup>a</sup>Parameters of this component kept frozen at values as described in the text.

<sup>b</sup>Emission Measure

<sup>c</sup>Index of absorbed power law fit

<sup>d</sup>Normalization of power law fit at 1 keV in units of photons  $\text{keV}^{-1} \text{ s}^{-1} \text{ cm}^{-2} \text{ sr}^{-1}$

Table 3.  $O_{VII}$  and  $O_{VIII}$  line intensities

Target	$O_{VII}$ ph s <sup>-1</sup> cm <sup>-2</sup> sr <sup>-1</sup>	$O_{VIII} K\alpha + O_{VII} K\beta$ ph s <sup>-1</sup> cm <sup>-2</sup> sr <sup>-1</sup>
<b>Mrk421-off-field1</b>	$5.5 \pm 0.9$	$1.4 \pm 0.5$
<b>Mrk421-off-field2</b>	$5.6 \pm 0.7$	$1.8 \pm 0.3$
<b>PKS2155-off-field1</b>	$7.4 \pm 0.7$	$1.9 \pm 0.4$
<b>PKS2155-off-field2</b>	$8.3 \pm 0.7$	$2.6 \pm 0.4$

## REFERENCES

- Anders, E. & Grevesse, N., *Geochimica et Cosmochimica Acta*, 53, 197A
- Anderson, M.E., Bregman, J. & Dai, X. 2013, *ApJ*, 762, 106
- Anderson, M.E. & Bregman, J. 2011, *ApJ*, 737, 22
- Anderson, M. & Bregman, J. 2010, *ApJ*, 714, 320
- Boylan-Kolchin et al. 2013, *ApJ*, 768, 140
- Bregman, J.N. 2007, *Ann. Rev. Astron. Astro.*, 45, 221
- Buote, D.A. et al. 2009, *ApJ*, 695, 135
- Cen, R., & Ostriker, J. P. 1999, *ApJ*, 514, 1
- Dai, X., Anderson, M.E., Bregman, J.N. & Miller, J.M. 2012, *ApJ*, 755, 107
- Dickey, J.M., & Lockman, F.J. 1990, *Ann. Rev. Astron. Astro.*, **28**, 215
- Ezoe, Y. et al. 2010, *PASJ*, 62, 981
- Fang, T.T. et al. 2012, *ApJ*, 762, 20
- Fang, T.T. et al. 2010, *ApJ*, 714, 1715
- Fang, T.T., Canizares, C.R., & Wolfire, M. 2006, *ApJ*, **644**, 174
- Feldmann, R., Hooper, D., Gnedin, N. Y. 2012, *ApJ*, 763, 21
- Fujimoto, R. et al. 2007, *PASJ*, 59S, 133
- Greevich, J. & Putman, M.E. 2009, *ApJ*, 696, 385
- Galeazzi, M. et al. 2013, in preparation
- Gupta, A. et al. 2009, *ApJ*, 707, 644
- Gupta, A., Mathur, S., Krongold, Y. et al. 2012, *ApJ*, 756L, 8
- Hagihara, T. et al. 2010, *PASJ*, 62, 723
- Henley, D.B. et al. 2010, *ApJ*, 723, 935
- Henley, D.B. & Shelton, R.L. 2012, *ApJS*, 202, 14

- Henley, D.B. & Shelton, R.L. 2013
- Hodges-Kluck, E.J. & Bregman, J.N. 2013, *ApJ*, 762, 12
- Humphrey, P.J. et al. 2011, *ApJ*, 729, 53
- Ishisaki, Y. et al. 2007, *PASJ*, 59, 113
- Kaastra, J.S. et al. 2006, 652, 189
- Koutroumpa, D. et al. 2009a, *ApJ*, 696, 1517
- Koutroumpa, D. et al. 2009b, *ApJ*, 697, 1214
- Koyama, K. et al. 2007, *PASJ*, 59S, 23
- Kuntz, K.D. & Snowden, S. 2000, *ApJ*, 543, 195
- Lallement, R. 2004, *Å*, 418, 143
- Lehner, N., & Howk, J.C. 2011, *Science*, 334, 955
- Lei, S., Shelton, R.L. & Henley, D.B. 2009, *ApJ*, 699, 1891
- Maller, A. H., & Bullock, J.S. 2004, *MNRAS*, 355, 694
- Mathur, S., Weinberg, D. & Chen, X. 2003, 2003, *ApJ*, 582, 82
- Mathur, S. et al. 2008, *Ap&SS*, 315, 93
- Mathur, S. 2012, arXiv1211.3137
- Mitsuda, K. et al. 2007, *PASJ*, 59S, 1
- Mitsuishi, I., Gupta, A., Yamasaki, N.Y. et al. 2012, *PASJ*, 64, 18
- Morrison, R. & McCammon, D. 1983, *ApJ*, 270, 119
- Nicastro, F., et al. 2002, *ApJ*, 573, 157
- Nicastro, F., et al. 2003, *nature*, 421, 719
- Nicastro, F., Mathur, S., Elvis, M. et al. 2005, *nature*, 433, 49
- Pedersen, K., Rasmussen, J., Sommer-Larsen, J. et al. 2006, *New Astronomy*, 11, 465
- Rasmussen, A., et al. 2009, *ApJ*, **697**, 79

- Sakai, K. et al. 2012, AIPC, 1427, 342
- Sembach, K. et al. 2003, ApJS, 146, 165
- Silk, J. 1977, ApJ, 211, 638
- Smith, R.K. & Cox, D.P. 2001, ApJS, 134, 283
- Smith, R.K. et al. 2007, PASJ, 59, 141
- Snowden, S.L. et al. 1998, ApJ, 493, 715
- Snowden, S.L. et al. 2000, ApJS, 128, 171
- Snowden, S. L., Collier, M. R. & Kuntz, K. D. 2004, ApJ, 610, 1182
- Sommer-Larsen, J. 2006, ApJ, 644, L1
- Tamura, T. et al. 2004, å, 420, 135
- Tawa, N. et al. 2008, PASJ, 60S, 11
- Toft, S., Rasmussen, J., Sommer-Larsen, J., & Pedersen, K. et al. 2002, MNRAS, 335, 799
- Tumlinson, J. et al. 2011, *Science*, 334, 948
- White, S.D.M., & Rees, M.J. 1978, MNRAS, 183, 341
- Williams, R.J. et al. 2013, ApJ, 762L, 10
- Williams, R.J., Mathur, S., Nicastro, F., & Elvis, M., 2007, ApJ, 665, 247
- Williams, R.J., Mathur, S. et al. 2006, ApJ, 645, 179
- Williams, R.J., Mathur, S. et al. 2005, ApJ, 631, 856
- Yao, Y., Wang, Q. D., Hagihara, T. et a. 2009, ApJ, 690, 143
- Yoshino, T. et al. 2009, PASJ, 61, 805
- Yoshitake, H. et al. 2013, PASJ, 65, 32
- Zappacosta, L. et al. 2012, ApJ, 753, 137

## A. Appendix

Here we show explicitly how a two component density distribution affects the resultant halo path-length and mass.

Let us assume that there is a high density component with  $n(High) = 1 \times 10^{-3} \text{ cm}^{-3}$  and pathlength  $L(High)=1\text{kpc}$ . We can identify this component with the Galactic disk, but that is not important. Let us also say there is a halo of density  $n(Low) = 1 \times 10^{-5} \text{ cm}^{-3}$ .

The column density of the high density component is then  $N_H = 3 \times 10^{18} \text{ cm}^{-2}$  and the emission measure  $EM(High)= n(High)^2 L(High) = 3 \times 10^{15}$  in units of  $\text{cm}^{-5}$ .

The EM would be strongly biased by the high density component, so let us assume it contributes 90% to the total emission measure. Therefore the total  $EM= 3.3 \times 10^{15}$  in the same units.

By construction, the EM from the low density component is only 10%, that is  $EM(Low)= 3.3 \times 10^{14}$  in the same units. Given this  $EM(Low)$  and  $n(Low)$  we can now calculate the path-length of the low density component:  $L(Low)= 300 \text{ kpc}$ . And its column density  $N_H(Low) = 3 \times 10^{19} \text{ cm}^{-2}$ .

The total disk + halo column density is then  $N_H = 3.3 \times 10^{19} \text{ cm}^{-2}$ . Thus we have completely defined a two component medium, with the high density component (disk) dominating the observed EM while the low density component (halo) dominating the observed column density. The EM we measure is  $EM= 3.3 \times 10^{15} \text{ cm}^{-5}$  and the total column density we measure is  $N_H = 3.3 \times 10^{19} \text{ cm}^{-2}$ .

If we now make the assumption of a single density medium, and derive density and pathlength from the total observed EM and  $N_H$ , the values we get are as follows. The average density is  $n = EM/N_H = 1 \times 10^{-4} \text{ cm}^{-3}$  and the average pathlength  $L= N_H/n = 110 \text{ kpc}$ . Thus, under the assumption of a single density plasma, the derived density is an order of magnitude higher and the derived pathlength is about a factor of three lower than the actual density and pathlength of the halo.

The actual mass of the halo (low density component) is  $M(Low)= n(Low)L(Low)^3 = 7.3 \times 10^{66}$  in dimensionless units (ignoring constants). The derived mass under the single component assumption, however, is  $M= nL^3 = 3.6 \times 10^{66}$  in the same dimensionless units. Thus the mass derived assuming a single density component is a factor of two lower than the actual mass.

Thus, the assumption of a single density halo underpredicts the halo pathlength and mass. We have explicitly presented a two component system here for simplicity, but it

shows that *any* density gradient would similarly strengthen our results. In this example, we have considered that the high density component contributes 90% to the total EM. Higher contribution to the EM would make the halo even more extended. We thus conclude that any disk contribution, clumping, and/or a declining density profile would make the halo more extended and more massive, thus strengthening our result.